Design and Optimization of Selective Protein Kinase C θ (PKCθ) Inhibitors for the Treatment of Autoimmune Diseases
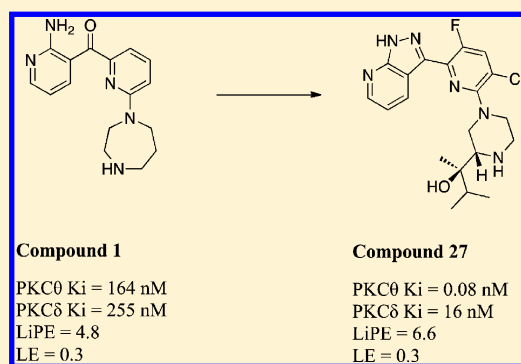
Juan-Miguel Jimenez,*,[†] Dean Boyall,[†] Guy Brenchley,[†] Philip N. Collier,[†] Christopher J. Davis,[†] Damien Fraysse,[†] Shazia B. Keily,[†] Jaclyn Henderson,[†] Andrew Miller,[†] Francoise Pierard,[†] Luca Settimo,[†] Heather C. Twin,[†] Claire M. Bolton,[‡] Adam P. Curnock,[‡] Peter Chiu,[‡] Adam J. Tanner,[‡] and Stephen Young[†]

[†]Department of Chemistry and [‡]Department of Biology, Vertex Pharmaceuticals (Europe) Ltd., 88 Milton Park, Abingdon, Oxfordshire OX14 4RY, U.K.

S *Supporting Information*

ABSTRACT: Protein kinase C θ (PKCθ) has a central role in T cell activation and survival; however, the dependency of T cell responses to the inhibition of this enzyme appears to be dictated by the nature of the antigen and by the inflammatory environment. Studies in PKCθ-deficient mice have demonstrated that while antiviral responses are PKCθ-independent, T cell responses associated with autoimmune diseases are PKCθ-dependent. Thus, potent and selective inhibition of PKCθ is expected to block autoimmune T cell responses without compromising antiviral immunity. Herein, we describe the development of potent and selective PKCθ inhibitors, which show exceptional potency in cells and in vivo. By use of a structure based rational design approach, a 1000-fold improvement in potency and 76-fold improvement in selectivity over closely related PKC isoforms such as PKCδ were obtained from the initial HTS hit, together with a big improvement in lipophilic efficiency (LiPE).

Compound 1

PKC0 Ki = 164 nM
PKCδ Ki = 255 nM
LiPE = 4.8
LE = 0.3

Compound 27

PKCθ Ki = 0.08 nM
PKCδ Ki = 16 nM
LiPE = 6.6
LE = 0.3

■ INTRODUCTION

Protein kinase C θ (PKCθ) is a member of a large family of serine/threonine kinases that are involved in diverse cellular functions. There are 11 PKC isoforms that can be subdivided into diacylglycerol- (DAG) and calcium-dependent classical isoforms (PKCs α, βI, βII, and γ), DAG-dependent novel isoforms (PKCs δ, ε, η, and θ), and DAG- and calcium-independent atypical isoforms (PKCs λ, ι, and ζ).[1] PKCθ expression is relatively restricted. The phenotype of the knockout mouse indicates a predominant role for this enzyme in T cells where it appears to play a central role in their activation by integrating signals from both the TCR (T cell receptor) and the co-stimulatory CD28.[2−4] During T cell activation, PKCθ is recruited to the center of the immune synapse (IS) where it is responsible for the activation of key transcription factors (AP-1, NFκB, and NFAT) that drive transcription of the IL-2 gene.[3−8] PKCθ also provides potent survival signals to T cells through the up-regulation of expression of the antiapoptotic molecules Bcl-xL and Bcl-2, as well as the inactivation of the proapoptotic molecule Bad.[9−12] PKCθ-deficient mice are able to mount a normal T cell response to certain pathogens, and their antiviral responses in particular appear to remain intact. These observations have obvious implications regarding the safety of drugs targeting this enzyme.[13−17] Interestingly, PKCθ appears to be essential for the development of T cell mediated inflammatory diseases

because PKCθ-deficient mice are resistant to or show markedly reduced symptoms in models of MS, IBD, arthritis, and asthma.[18−23]

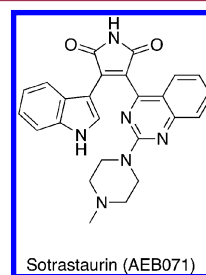The Novartis pan-PKC inhibitor sotrastaurin (AEB071) (Figure 1) is currently in phase II clinical studies for

Figure 1. Structure of pan PKC inhibitor from Novartis.

transplantation and psoriasis.[24,25] Sotrastaurin is a potent inhibitor of both novel and classical PKC isoforms (IC$_{50}$: PKCθ 1 nM, PKCδ 1.3 nM, PKCα 2.1 nM, PKCβI 2 nM).[26] Its potent inhibition of PKC isoforms involved in B cell and T cell function (PKCα, PKCβ, and PKCθ) results in a level of immunosuppression that makes it suitable for use in trans-

Scheme 1[a]
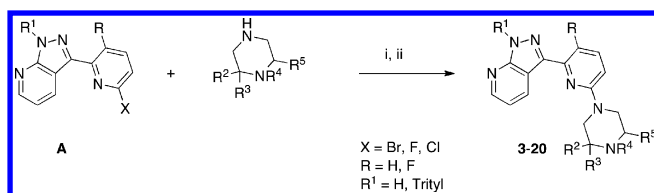
^{a}(i) Base, 110−190 °C, solvent; (ii) TFA, Et$_3$SiH, DCM, rt.

plantation.[26,27] In the treatment of autoimmune diseases, it is anticipated that selective inhibition of PKCθ will provide a better balance of efficacy and safety by inhibiting autoimmune T cell responses without causing overt immunosuppression. Such an approach has found significant favor within the pharmaceutical industry; however, while some companies have reported promising preclinical data, there are no selective PKCθ inhibitors reported to be in clinical trials.[28−40]

As part of our own program to identify potent and selective PKCθ inhibitors, we identified compound **1** as an interesting hit from HTS of the Vertex corporate compound collection.[41] Compound **1** has a low molecular weight (297.16), good physicochemical properties with acceptable lipophilicity (cLogP = 2), and good PKCθ potency, which result in good ligand and lipophilic efficiency (LE = 0.3, LiPE = 4.8) (Figure 2).[42] The compound, however, displays poor selectivity over PKCδ, an enzyme that when knocked out in mice causes a fatal B cell autoimmunity syndrome.[43,44] Compound **1** also showed modest selectivity over PKCα as a representative isoform of the classical subfamily. It was quickly established that replacement of the diazepane with a piperazine ring (**2**) improved PKCθ potency approximately 5-fold and improved the lipophilic efficiency (LiPE = 5.5). This was desirable, since substituted piperazines are both more commercially and synthetically accessible and would allow us to explore the SAR around the piperazine more easily. We also realized that transformation of the aminopyridine ketone hinge-binding motif into a 3-pyrazolo[3,4-b]pyridine (**3**) resulted in a trend toward enhanced selectivity for PKCθ over both novel and classical PKC isoforms while maintaining a good level of lipophilic efficiency. Maintaining a good level of lipophilic efficiency was deemed important, as kinase inhibitors are notoriously bad in gaining potency through unspecific lipophilic interactions[45] and there is an increasing body of evidence

suggesting that development candidates with high lipophilic efficiency (LiPE of 5−7) are more likely to succeed.[42] The addition of a fluorine substitution in the 5-position of the pyridine central ring was also well tolerated (**4**). Encouraged by this data and the overall kinase selectivity offered by these lead compounds (data not shown), we decided to initiate our lead optimization campaign.

■ CHEMISTRY

Scheme 1 outlines the versatile synthetic sequence developed to both fully explore the effects of substitution around the piperazine ring and install a diverse set of substituted piperazines as a final step on both the unsubstituted and F-substituted central rings.

Pyridylpyrazolopyridines **A** were prepared (see Materials and Methods and Supporting Information) and reacted with the appropriate piperazine using a range of bases and solvents under microwave conditions. In the case of the trityl protected 3-pyrazolopyridine and Boc protected piperazines, a final TFA mediated deprotection afforded the desired products (**3−20**).

Schemes 2 and 3 highlight the synthetic routes used to explore effects of the substitution in the central pyridine ring. Trisubstituted pyridylpyrazolopyridines (**D**) were constructed from either the Weinreb amide (**B**) or pyrazolopyridine (**E**) as shown in Scheme 2. Nucleophilic addition of an anion derived from a suitable pyridine derivative to Weinreb amide (**B**) gave dipyridyl ketone (**C**) which was ring closed with hydrazine to pyridylpyrazolopyridine (**D**). Alternatively, suitable protection of 3-bromo-1H-pyrazolo[3,4-b]pyridine (**E**) and formation of the pyrazolopyridine boronic ester (**G**) allowed the pyridine central ring to be installed by a Suzuki cross-coupling to provide pyridylpyrazolopyridine (**D**).

To access tetrasubstituted pyridine derivatives, it was necessary to control the regiochemistry on a polysubstituted pyridine ring. The route described above was therefore modified to allow introduction of 3,5-substituted derivatives. Deprotonation of 3-chloro-2,5-difluoropyridine (**H**) occurs preferentially in the 4-position, and it was necessary to introduce a transient substituent to block this position to allow selective coupling of the pyridine with Weinreb amide (**B**) at the 2-position. Scheme 3 illustrates this with the route to the 3-chloro-5-fluoro derivatives. Deprotonation of 3-chloro-2,5-difluoropyridine (**H**) and quenching with TBSCl introduced a TBS group at the 4-position to provide 4-(*tert*-

Scheme 2[a]
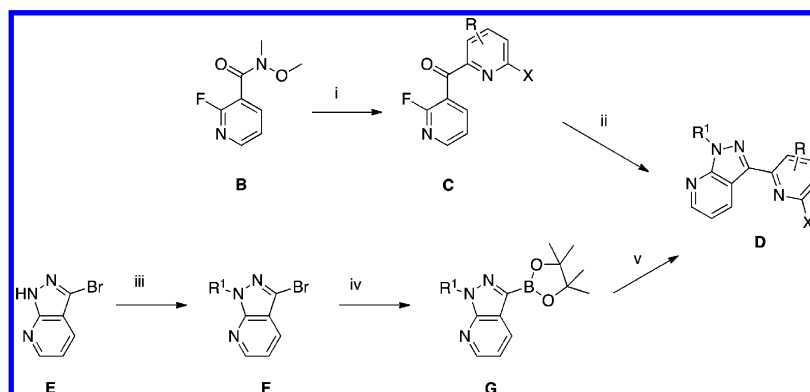
^{a}(i) Pyridine derivative, base; (ii) NH$_2$NH$_2$, solvent; (iii) protection; (iv) bis(pinacolato)diboron, PdCl$_2$(dppf)·DCM, KOAc, DMF, heat; (v) Pd(PPh$_3$)$_4$, Na$_2$CO$_3$, toluene, ethanol, water, heat, pyridine derivative.
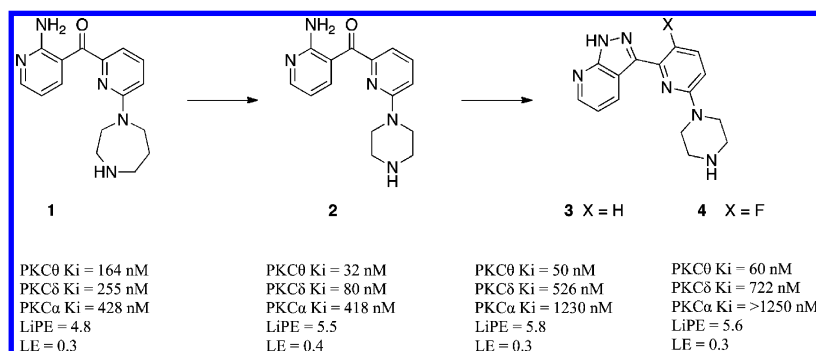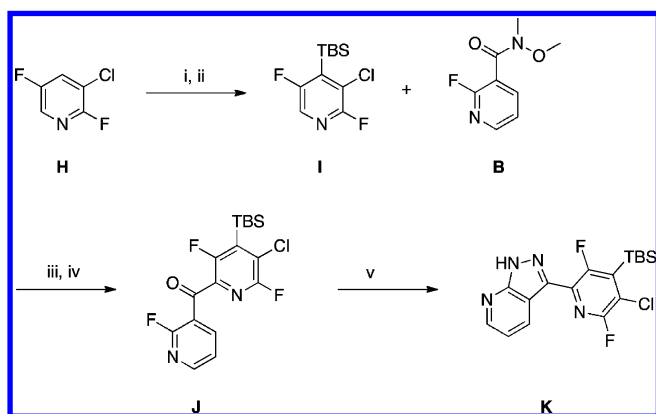
Figure 2.

Scheme 3[a]

[a](i) Diisopropylamine, *n*-BuLi, THF, −78 °C; (ii) TBSCl, −78 °C, 72%; (iii) diisopropylamine, *n*-BuLi, THF, −85 °C; (iii) Weinreb amide, 95%; (iv) NH₂NH₂, dioxane, CaCO₃, −10 °C to rt, 98%.

Figure 3. Proposed binding mode of compounds **3** (yellow) and **4** (blue) in PKCθ (green) showing the surface defined in the ATP active site. Within the C-terminus loop, there is a significant difference of a cysteine in PKCθ to a larger tyrosine in PKCδ (brown). Phe664 (C-terminus loop) and Leu386 (GRL) (green) create a bigger hydrophobic pocket in PKCθ as compared with Phe633 and Leu355 (brown) in PKCδ.

butyldimethylsilyl)-3-chloro-2,5-difluoropyridine (**I**). A second deprotonation at the 2-position and reaction with Weinreb amide (**B**) gave dipyridyl ketone (**J**), and the usual closure with hydrazine provided pyrazolopyridine (**K**).

The synthesis of key intermediates **D** and **K** allowed easy introduction of the piperazine moiety at a late stage and a series of simple deprotections, as described in Materials and Methods and Supporting Information, provided access to the compounds as reported in Table 3.

■ **RESULTS AND DISCUSSION**

Good selectivity over PKCδ was considered to be crucial, so we aimed to address this early in the optimization process. Initial analysis based upon amino acid sequence suggested that the ATP active sites of both these isoforms are highly conserved with a single residue difference (Tyr108 in PKCθ and Phe108 in PKCδ). However, analysis of the crystal structures of human PKCθ, reported by Novartis, in complex with both staurosporine and 3-(8-((dimethylamino)methyl)-6,7,8,9-tetrahydropyrido[1,2-*a*]indol-10-yl)-4-(1-methyl-1*H*-indol-3-yl)-1*H*-pyrrole-2,5-dione (PDB code 2JED) showed the C-terminus in close contact with the ligand.[46] A homology model of PKCδ was built based upon this structure of PKCθ and showed that within the C-terminus there is a significant difference of a Cys661 in PKCθ to a larger Tyr630 in PKCδ (Figure 3).[46] The consequence of this residue difference is the presence of a bigger hydrophobic pocket in PKCθ as compared to PKCδ that might be exploitable to gain potency and selectivity (see Figure 3). On the basis of docking and
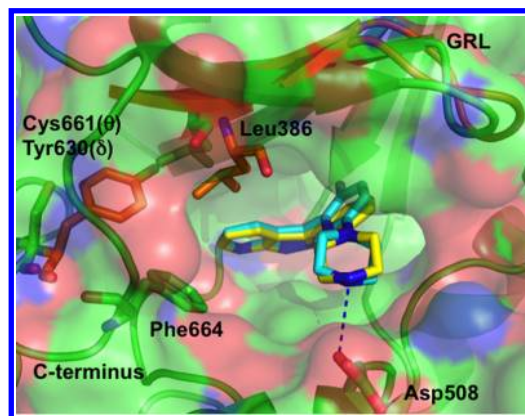
minimization of our scaffold, we realized that we could access this pocket from the piperazine ring. So we set out to exploit this difference to affect δ/θ selectivity and PKCθ potency (Table 1).
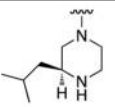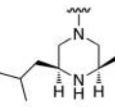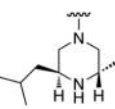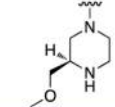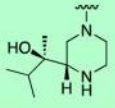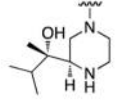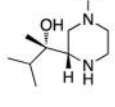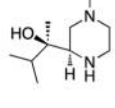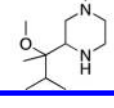
Table 1. Structures and Inhibitory Activity of Compounds 3−12[a]

compd	X	R¹	PKCθ K_i[b] (nM)	PKCδ K_i[b] (nM)	δ/θ
3	H	H	50	526	10
5	H	(*R*)-Me	68	336	5
6	H	(*R*)-Et	12	81	7
7	H	(*S*)-ⁱPr	15	132	9
8	H	(*R*)-ⁱBu	5	131	27
9	H	(*S*)-ⁱBu	2	89	45
10	H	(*R*)-Ph	5	151	27
11	F	(*R*)-ⁱBu	9	792	88
12	F	(*S*)-ⁱBu	4	358	90

[a]Functionalization at the 2-position of piperazine and central pyridine ring. [b]Mean from $n \geq 2$ independent experiments.

Table 2. Structures and Inhibitory Activity of Piperazine Derivatives 12−20

Compounds	R^1	cLogP	PKCθ Ki^a (nM)	PKCδ Ki^a (nM)	δ/θ	LipE
12		3.4	4	358	90	5.0
13		3.8	5	130	26	4.5
14		3.8	>700	>1250	–	–
15		2.0	51	>1250	>25	5.3
16		2.7	0.2	57	285	6.8
17		2.7	133	>1250	>10	4.0
18		2.7	1	120	120	6.1
19		2.7	21	>1250	>60	4.8
20		3.4	10	480	48	4.2

^{a}Mean from $n \geq$ of 2 independent experiments.

To the unsubstituted pyridine central ring (3), the introduction of simple lipophilic substituents in the 2-position of the piperazine ring resulted in a size dependent increase in PKCθ potency by up to 25-fold (9), which is consistent with filling a hydrophobic pocket. There was no obvious preference for the S-stereochemistry around the piperazine ring (8 vs 9). The larger lipophilic groups (Ph and ^{i}Bu) also provided better selectivity over PKCδ (up to 45-fold), consistent with the proposed model. Although it had little impact on potency, introduction of fluorine into the central ring further enhanced selectivity over PKCδ (11 and 12) up to 90-fold. This enhancement is possibly a consequence of a greater torsion angle between the central pyridine ring and the hinge binder, which subtly repositions the lipophilic substituent on the piperazine ring resulting in a greater clash in PKCδ (Figure 3).

As such, compounds bearing fluorine on the central ring were considered the most attractive leads because they combined a good PKCθ potency, high lipophilic efficiency, and enhanced δ/θ selectivity (90-fold).

With this encouraging selectivity, we set out to explore the SAR around the piperazine ring in more detail, with the view to improving PKCθ potency while maintaining good selectivity over PKCδ (Table 2).

2,6-Disubstituted piperazines did not provide an increase in potency, were detrimental to selectivity, and demonstrated a large difference in potency between the R- and S-methylated piperazines (13 and 14). Introduction of a tertiary alcohol in the side chain showed an increase in PKCθ enzyme inhibition, providing a 200 pM K_i inhibitor of PKCθ (16). The significant improvement in LiPE (6.8) highlighted the fact that the

increase in potency is being driven by improvements in key polar interactions. In addition, there was a significant increased selectivity over PKCδ (285-fold). This piperazine alcohol is believed to form a bidentate hydrogen bond network with the Asp508, which locks the molecule in a conformation that places the isopropyl group in the hydrophobic pocket created by the C-terminus and GRL (see Figure 4). The stereochemistry at
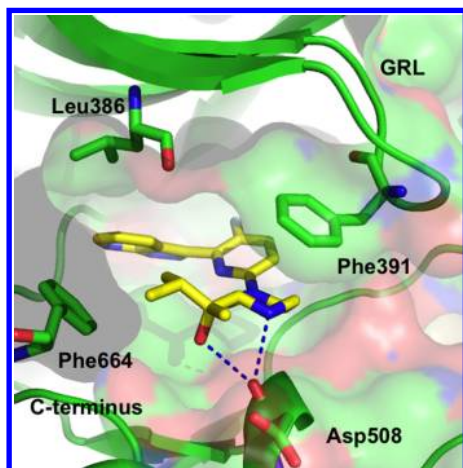

Figure 4. Predicted binding mode of compound **16** in PKCθ showing the proposed bidentate hydrogen-bonding network between the secondary amine and hydroxyl group, with the main chain carbonyl oxygen of Asp 508. Correct positioning of both the H-bond and lipophilic isopropyl group is crucial to obtain exquisite PKCθ potency and good selectivity over PKCδ.
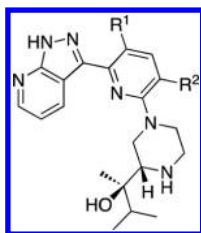
both the piperazine ring and the tertiary alcohol center is important to attain this exquisite potency and selectivity. The S-stereochemistry at the piperazine (**16** vs **19**) and the R-stereochemistry of the alcohol (**16** vs **18**) best orientate the

isopropyl upward into the lipophilic pocket. Methylation of the alcohol (**20**, mixture of all four isomers) confirmed that the alcohol was likely acting as a hydrogen bond donor and forming an integral part of the bidentate H-bond network (0.2 nM compared to 10 nM).

With the piperazine alcohol **16** providing very good potency and selectivity, we turned our attention back to the pyridine central ring because the model suggested that there was an adjacent pocket that could be accessed to further improve potency. However, substitutions bigger than fluorine in R^1 was not well tolerated and resulted in a significant loss in PKCθ affinity (**21** and **22**) (Table 3). Similarly, substitution in position 4 of the pyridine was not beneficial for potency or selectivity (data not shown). Introduction of polarity at R^2 had either a detrimental effect on PKCθ potency (**24**) or selectivity over PKCδ (**23** and **25**). The presence of a 3-fluoro-5-fluoro and 3-chloro-5-fluoro substitution (**26** and **27**) provided a 100 and 80 pM PKCθ potency, respectively, with good selectivity over PKCδ of approximately 200-fold. Compounds in this series in general showed a good translation into potency in a cell-based assay, as measured by inhibition of IL-2 in stimulated PBMCs. In particular, compounds **16**, **23**, **25**, **26**, and **27** showed impressive potency in a cell-based assay in the low nanomolar range (Table 3).

On the basis of the PKCθ potency, selectivity over PKCδ, and excellent potency in a cell-based assay, compounds **16**, **26**, and **27** were characterized further. The impressive potency in our cell based IL-2 assay observed for these compounds translated into good potency in the more physiologically relevant whole blood IL-2 assay (WB IL-2) with values in the range 100−200 nM (Table 4). Table 4 also summarizes their pharmacokinetic properties in rat. Compounds **16** and **26** demonstrate a modest oral bioavailability despite a low plasma clearance of compound **26**. Compound **27** showed the best PK

Table 3. Structures and Inhibitory Activity of Substituted Central Pyridine Derivatives 16 and 21−27

Compounds	R$_1$	R$_2$	PKCθ Ki[a] (nM)	PKCδ Ki[a] (nM)	PKCα Ki[a] (nM)	IL-2 IC$_{50}$ (nM)
16	F	H	0.2	57	549	6[a]
21	Cl	H	21	547	1240	170[b]
22[c]	CF$_3$	H	20	957	>1250	420[b]
23	F	OH	0.1	<10	56	4[b]
24	F	CN	1	242	>1250	120[b]
25	F	CH$_2$OH	0.1	<10	205	1[b]
26	F	F	0.1	18	198	2[a]
27	F	Cl	0.08	16	356	11[a]

[a]Mean from $n \geq 2$ independent experiments. [b]Data from $n = 1$. [c]Racemic.

Table 4. Overall Profile of Lead Compounds 16, 26, and 27
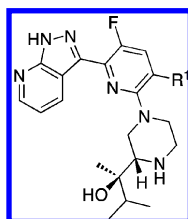
compd	R[1]	PKCθ K_i^{a} (nM)	PKCδ K_i^{a} (nM)	PKCα K_i^{a} (nM)	IL-2 IC$_{50}$^{a} (nM)	WB IL-2 IC$_{50}$^{a} (nM)	rat PK^b CL (mL min^{-1} kg^{-1})	$t_{1/2}$ (h)	F (%)
16	H	0.2	57	549	6	200	39	2.6	36
26	F	0.1	18	198	2	80	9.5	1.7	30
27	Cl	0.08	16	356	11	70	7	4.7	65

^{a}Mean from $n \geq 2$ independent experiments. ^{b}Rat PK reported (iv bolus 3 mg/kg and po dose of 10 mg/kg). Data reported as an average of three animals.

Table 5. Selectivity Profile for Compound 27
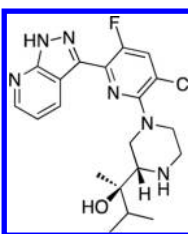
Enzymes in the TCR pathway	K_i^{a} (nM)	PKC subclass	Isoform	K_i^{a} (nM)
PKCθ	0.08	Classical	α	356
Lck	>1000		βI	15
Itk	>1000		βII	393
Fyn	>1000		γ	725
Lyn	>1000	Novel	δ	16
Zap70	>1000		ϵ	1
c-Raf	>1000		θ	0.08
Erk-1	>1000		η	3.5
		Atypical	μ	2420
			ζ	>5000

^{a}Mean from $n \geq 2$ independent experiments.
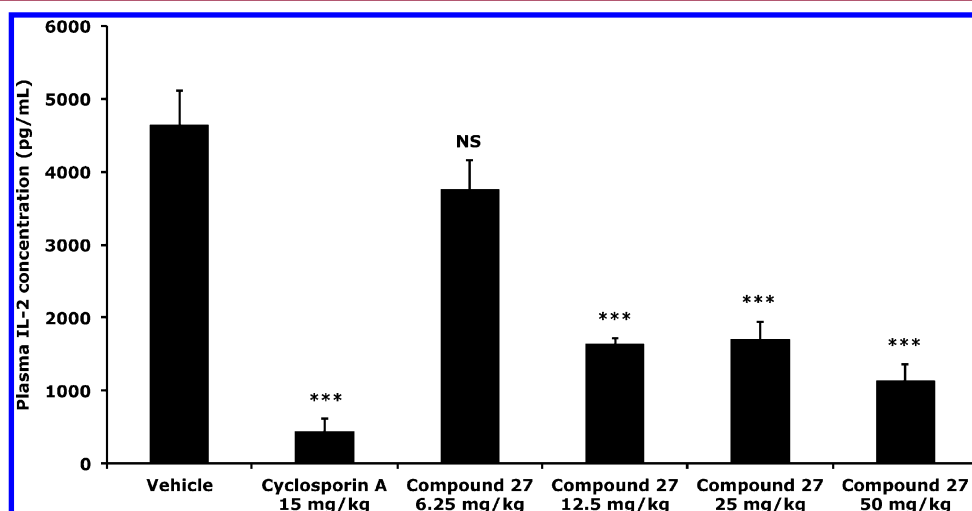
Figure 5. In vivo data for **27** in the SEB IL-2 model. Each column represents a mean ± SEM ($n = 6-8$). Statistical analysis of data was conducted with a one-way ANOVA followed by a Dunnett's post-test: (∗∗∗) $p < 0.001$, and NS denotes no significant effect compared to the vehicle control group.

profile with a low clearance (7 mL min^{-1} kg^{-1}), long half-life (4.7 h), and good oral bioavailability (65%).

Compound **27** possessed excellent overall characteristics and was selected for further characterization. Importantly, this compound did not show cross-reactivity against other proximal TCR kinases such as Src kinases, Syk kinases, Tec kinases, or MAP kinases (Table 5). Good selectivity was also seen against other PKC family members, particularly classical isoforms (>1000-fold except PKCβ I, 200-fold) and atypical isoforms (>10000-fold). As anticipated, attaining selectivity over the more closely related novel PKC family members was more challenging, with a good 200-fold being achieved over PKCδ (Table 5). This was perceived as especially important because of the risk of B cell autoimmunity associated with inhibition of the PKCδ isoform. Extended tests were conducted to examine the cross-reactivity profiles of these compounds against a diverse range of enzymes, receptors, and ion channels. Again, excellent selectivity over non-kinase targets was seen (data not shown). Because of the promising overall profile, compound **27** was selected for in vivo evaluation in a murine model of staphylococcal enterotoxin B induced IL-2 release (SEB IL-2 model) (Figure 5 and experimental section for details). A single dose of **27** was administered orally at 6.25, 12.5, 25, and 50 mg/kg (e.g., at 25 mg/kg C_{max} concentration 700 ng/mL) and demonstrated potent dose dependent inhibition of IL-2 production (Figure 5).

■ CONCLUSION

In summary, the design and optimization of a novel class of potent and selective PKCθ inhibitors based on the pyrazolo-[3,4-b]pyridine scaffold have been described. Compound **27** is a potent and selective inhibitor of the PKCθ enzyme with an excellent overall profile, where a 1000-fold improvement in potency and 76-fold improvement in selectivity over closely related PKC isoforms such as PKCδ were obtained compared with the initial HTS hit. In addition, a significant improvement in lipophilic efficiency (LiPE) was achieved, indicating that our lead candidate improves nonlipophilic interactions with the PKCθ enzyme. Accessing these key interactions enabled us to precisely position the molecule to capitalize on subtle differences between closely related PKC isoforms that have almost identical ATP binding sites. On the basis of its favorable physicochemical and ADMET properties, compound **27** was selected for further evaluation in disease models of MS and IBD. These studies will be the subject of further communications from this laboratory.

■ MATERIALS AND METHODS

General Experimental Details. All commercially available solvents and reagents were used as received. Microwave reactions were carried out using a CEM Discovery microwave. Analytical thin layer chromatography was carried out using glass-backed plates coated with Merck Kieselgel 60 GF240. Plates were visualized using UV light (254 or 366 nm) and/or by staining with potassium permanganate followed by heating. Flash chromatography was carried out on an ISCO Combiflash Companion system, eluting with a 0−100% EtOAc/petroleum ether gradient. Samples were applied preabsorbed on silica. Where stated, purification was performed using a Waters FractionLynx HPLC mass directed instrument using an appropriate acetonitrile/water gradient with either TFA or ammonia modifier. Where stated, supercritical fluid chromatography (SFC) was performed on a Berger Minigram SFC machine. ^{1}H NMR and ^{19}F NMR spectra were recorded at 400 and 376 MHz, respectively, using a Bruker DPX 400 instrument. MS samples were analyzed on a MicroMass Quattro Micro

mass spectrometer operating in single MS mode with electrospray ionization. Samples were introduced into the mass spectrometer using chromatography. The melting points were determined on a Mettler Toledo DSC1 STAR system, calibrated using indium. All final products had a purity of >95%. The purity of final products was determined by HPLC or combustion analyses. HPLC purity was measured on an Agilent HP1100 HPLC instrument with a Waters Quattro MS system equipped with an ACE C8 reverse phase column (4.6 mm × 150 mm, 5 μm). The mobile phases were acetonitrile/methanol (1:1) and water (20 mM, pH 7.0, Tris phosphate). Combustion analyses were performed on a Control Equipment Corporation 440 elemental analyzer.

3-(6-(Piperazin-1-yl)pyridin-2-yl)-1H-pyrazolo[3,4-b]pyridine (3). *Step 1.* A solution of 2-(dimethylamino)ethanol (3.53 g, 3.98 mL, 39.63 mmol) in hexane (45 mL) cooled to −78 °C under N$_2$ was treated with n-BuLi (31.70 mL of 2.5 M, 79.26 mmol), and the reaction mixture was allowed to stir for 20 min. A solution of 2-chloropyridine (1.50 g, 13.21 mmol) in hexane (12 mL) was added dropwise and the resultant orange solution stirred for a further 50 min. The mixture was then treated dropwise with a solution of 2-fluoro-N-methoxy-N-methylpyridine-3-carboxamide (9.25 g, 50.20 mmol) in THF (15 mL) to give a deep-orange suspension. Stirring became difficult at this stage, and a further 8 mL of THF was added. The reaction mixture was kept at −78 °C for 1 h, quenched with saturated aqueous NH$_4$Cl, and then diluted with EtOAc. The mixture was allowed to warm to room temperature. The aqueous layer was extracted further with EtOAc, and the combined organics were washed with saturated aqueous NaHCO$_3$ solution followed by brine. The mixture was dried over MgSO$_4$ and concentrated to give an orange residue, which was purified by column chromatography (ISCO Companion, 80 g column, compound preabsorbed onto silica), eluting with 5−100% EtOAc/petroleum ether to afford (6-chloropyridin-2-yl)-(2-fluoropyridin-3-yl)methanone as an off-white solid (1.17 g, 37.4%). ^{1}H NMR (CDCl$_3$) δ 7.37 (1H, m), 7.57 (1H, t), 7.93 (1H, m), 8.05 (1H, m), 8.21 (1H, t), 8.45 (1H, m). MS m/z: 236.9 (M + H)$^+$.

Step 2. A solution of (6-chloro-2-pyridyl)(2-fluoro-3-pyridyl)-methanone (307 mg, 1.30 mmol) in THF (2.5 mL) was treated with hydrazine (1.0 M in THF) (1.30 mL of 1 M, 1.30 mmol), and the mixture was heated in the microwave at 100 °C for 60 min. The reaction mixture was concentrated in vacuo to give 3-(6-chloropyridin-2-yl)-1H-pyrazolo[3,4-b]pyridine as a yellow solid (288 mg, 86.6%). ^{1}H NMR (DMSO-d_6) δ 7.35 (1H, m), 7.52 (1H, m), 8.01 (1H, t), 8.17 (1H, m), 8.61 (1H, m), 8.81 (1H, m), 14.11 (NH). MS m/z: 230.9 (M + H)$^+$.

Step 3. A mixture of 3-(6-chloropyridin-2-yl)-1H-pyrazolo[3,4-b]pyridine (60 mg, 0.26 mmol) and piperazine (112 mg, 1.30 mmol) was heated in a microwave at 190 °C for 90 min. The crude material was purified on FractionLynx and freeze-dried to afford compound **3** bis-TFA salt as a yellow solid (75.5 mg, 57%). ^{1}H NMR (DMSO-d_6) δ 3.30 (4H, s), 3.84 (4H, t), 6.96 (1H, d), 7.31 (1H, dd), 7.58 (1H, d), 7.73−7.77 (1H, m), 8.58 (1H, dd), 8.79 (1H, dd), 8.82 (2H, s), and 13.89 (1H, s). MS m/z: 281.0 (M + H)$^+$.

(R)-3-(3-Fluoro-6-(3-isobutylpiperazin-1-yl)pyridin-2-yl)-1H-pyrazolo[3,4-b]pyridine (11). *Step 1.* A suspension of diazabicyclo[2.2.2]octane (32.2 g, 0.29 mol) in dry TBME (365 mL) was cooled to −78 °C. n-BuLi (2.5 M in hexane, 0.29 mol) was added dropwise to the suspension. The mixture was stirred for approximately 30 min at −78 °C and then treated dropwise with 2,5-difluoropyridine (30.0 g, 0.26 mol) in dry TBME (15 mL). After 1 h, 2-fluoro-N-methoxy-N-methylnicotinamide (52.8 g, 0.29 mol) in dry TBME (30 mL) was added dropwise to the mixture at −78 °C. The solution was stirred for 1 h, and the reaction was quenched with saturated aqueous NH$_4$Cl (300 mL). The mixture was diluted with EtOAc (600 mL) and allowed to warm to room temperature overnight. The aqueous phase was extracted further with EtOAc (3 × 300 mL), and the combined organic phases were washed with saturated aqueous NaHCO$_3$ (500 mL) and brine (500 mL), dried over MgSO$_4$, and concentrated under reduced pressure to afford (3,6-

difluoropyridin-2-yl)(2-fluoropyridin-3-yl)methanone as a yellow/orange solid (66.7 g, 97%).

Step 2. To a solution of (3,6-difluoropyridin-2-yl)(2-fluoropyridin-3-yl)methanone) (66.7 g, 0.26 mol) in THF (450 mL) was added hydrazine hydrate (12.2 g, 0.38 mol). The mixture was stirred for 1 h at room temperature and then treated with another batch of hydrazine hydrate (12.2 g, 0.38 mol). The mixture was stirred overnight at room temperature, diluted with H_2O (200 mL), and stirred for 10 min. The product was isolated by filtration, washed with Et_2O, and dried under reduced pressure to afford 3-(3,6-difluoropyridin-2-yl)-1*H*-pyrazolo-[3,4-*b*]pyridine as a white solid (33.6 g, 55.5%). ^{1}H NMR (DMSO-*d*$_6$) δ 7.33 (1H, dt), 7.36 (1H, dd), 8.15 (1H, td), 8.62 (1H, dd), 8.71 (1H, brs), 9.15 (1H, brs). MS *m*/*z*: 233.8 (M + H)$^+$.

Step 3. A mixture of 3-(3,6-difluoropyridin-2-yl)-1*H*-pyrazolo[3,4-*b*]pyridine (100 mg, 0.43 mmol), (*R*)-2-isobutylpiperazine-bis-TFA salt (202 mg, 0.55 mmol), and DIPEA (235 mg, 1.82 mmol, 2.5 mL) was heated in a microwave at 185 °C for 40 min. The crude material was purified on FractionLynx and freeze-dried to afford compound **11** as a white solid (20.0 mg, 13%). MS *m*/*z*: 355.1 (M + H)$^+$.

(*R*)-2-((*S*)-4-(3,5-Difluoro-6-(1*H*-pyrazolo[3,4-*b*]pyridin-3-yl)-pyridin-2-yl)piperazin-2-yl)-3-methylbutan-2-ol (26). *Step 1.* A solution of diisopropylamine (98.9 g, 136.9 mL, 976.9 mmol) in THF (1.35 L) was cooled to −65 °C. *n*-BuLi (2.5 M in hexanes) (375.8 mL of 2.5 M, 939.4 mmol) was added dropwise via cannula over 1 h at such a rate as to maintain reaction temperature below −60 °C. Once the addition was completed, the cooling bath was removed and the reaction mixture was allowed to warm to 0 °C. The reaction mixture was stirred for 15 min at 0 °C, then recooled to −78 °C. 2,3,5-Trifluoropyridine (100.0 g, 751.5 mmol) was added dropwise via cannula over 20 min at such a rate to maintain the reaction temperature below −69 °C. The reaction mixture was stirred for 45 min at −78 °C during which time the solution turned orange/brown. A solution of *tert*-butylchlorodimethylsilane (147.2 g, 976.9 mmol) in THF (150 mL) was then added via cannula over 30 min. The reaction mixture was stirred at −78 °C for 90 min during which time the solution darkened. A saturated aqueous NH_4Cl solution (300 mL) was added, and the mixture was allowed to warm to room temperature. The reaction mixture was diluted with water (100 mL) and extracted with EtOAc (1.5 L, then 2 × 500 mL). The combined organics were washed with saturated aqueous $NaHCO_3$ (500 mL) and brine (400 mL). The crude mixture was partially concentrated in vacuo, dried ($MgSO_4$), and concentrated in vacuo. The material was purified by flash chromatography (CombiFlash Companion XL, 1.5 kg column, 0−20% EtOAc in petroleum ether) to afford 4-(*tert*-butyldimethylsilyl)-2,3,5-trifluoropyridine as a colorless oil (136.2 g, 73%). ^{1}H NMR (CDCl$_3$) δ 0.34 (6H, s), 0.89 (9H, s), 7.73 (1H, s). MS *m*/*z*: 248.1 (M + H)$^+$.

Step 2. A solution of diisopropylamine (66.78 g, 92.49 mL, 659.9 mmol) in THF (1.36 L) was cooled to −20 °C under nitrogen. *n*-BuLi (2.5 M in hexane) (253.0 mL of 2.5 M, 632.4 mmol) was added dropwise via cannula at such a rate as to maintain the internal temperature below −15 °C. The solution was warmed to 0 °C, then immediately recooled to −90 °C. *tert*-Butyldimethyl-(2,3,5-trifluoro-4-pyridyl)silane (136 g, 549.9 mmol) was added dropwise via cannula at such a rate as to maintain the internal temperature below −85 °C. After complete addition, the reaction mixture was stirred at −85 °C for 1 h and then 2-fluoro-*N*-methoxy-*N*-methylpyridine-3-carboxamide (116.5 g, 632.4 mmol) was added dropwise over 1 h, keeping the internal temperature below −85 °C. The mixture was stirred at −85 °C for 45 min. The cooling bath was removed and the mixture warmed to −50 °C. A saturated ammonium chloride aqueous solution (300 mL) was added and the mixture allowed to warm to room temperature. The mixture was diluted with EtOAc (2.5 L). The aqueous phase was separated and extracted with EtOAc (500 mL). The combined organics were washed with brine and partially concentrated in vacuo. The solution was dried ($MgSO_4$), filtered, and concentrated in vacuo to yield a brown oil. The material was purified on silica gel, eluting with 0−20% EtOAc in petroleum ether to afford (4-(*tert*-butyldimethylsilyl)-3,5,6-trifluoropyridin-2-yl)(2-fluoropyridin-3-yl)methanone as a yellow oil which solidified on standing

(159.6 g, 78%). ^{1}H NMR (CDCl$_3$) δ 0.35 (6H, s), 0.88 (9H, s), 7.29 (1H, m), 8.13 (1H, m), 8.37 (1H, m); ^{19}F NMR (decoupled) δ −112.47, −106.7, −89.3, −61.95.

Step 3. [4-[*tert*-Butyl(dimethyl)silyl]-3,5,6-trifluoro-2-pyridyl]-(2-fluoro-3-pyridyl)methanone (159 g, 429.2 mmol) was dissolved in dioxane (1.6 L), and calcium carbonate (85.91 g, 858.4 mmol) was added to the solution. The reaction mixture was stirred in an ice bath, and hydrazine hydrate (107.4 g, 104.4 mL, 2.15 mol) was added dropwise over 30 min. The resultant mixture was stirred for 18 h, gradually warming to room temperature. The reaction mixture was filtered through a pad of Celite, washing with EtOAc/MeOH 7:1 (2 × 500 mL) and water (100 mL). The filtrate was partitioned between EtOAc (1 L) and water (500 mL). The organic phase was washed with a saturated aqueous $NaHCO_3$ solution (500 mL). The combined aqueous layers were extracted with EtOAc (2 × 200 mL). The combined organics were washed with brine (400 mL), dried ($MgSO_4$), and concentrated to give an orange solid. The solid was triturated with DCM and filtered, washing with DCM and petroleum ether. The filtrate was concentrated under reduced pressure, and the resulting solid was again triturated and filtered, washing with more petroleum ether. The solids were combined to afford 3-(4-(*tert*-butyldimethylsilyl)-3,5,6-trifluoropyridin-2-yl)-1*H*-pyrazolo[3,4-*b*]pyridine as an off-white solid (140.5 g, 90%). ^{1}H NMR (CDCl$_3$) δ 0.55 (6H, s), 1.02 (9H, s), 7.21 (1H, m), 8.69 (1H, m), 8.91 (1H, s), 11.69 (1H, brs). MS *m*/*z*: 365.2 (M + H)$^+$.

Step 4. A 500 mL glass pressure vessel was charged with 3-(4-(*tert*-butyldimethylsilyl)-3,5,6-trifluoropyridin-2-yl)-1*H*-pyrazolo[3,4-*b*]-pyridine (26.80 g, 73.53 mmol), a mixture of (*R*)-3-methyl-2-((*S*)-piperazin-2-yl)butan-2-ol and (*R*)-3-methyl-2-((*R*)-piperazin-2-yl)-butan-2-ol (19.0 g, 110.3 mmol), THF (53 mL), and imidazol-1-yltrimethylsilane (51.57 g, 53.72 mL, 367.7 mmol). An identical experiment was run in parallel. The containers were sealed, and the mixture was heated and stirred at 95 °C for 18 h. Analysis of the crude reaction mixture showed a mixture consisting of 73% of the desired (*R*,*S*)-diastereoisomer and 18% of the (*R*,*R*)-diastereoisomer. Both reaction mixtures were cooled, combined, and diluted with EtOAc (500 mL). The solution was washed with saturated aqueous $NaHCO_3$ (2 × 200 mL). The combined aqueous layers were extracted three times with EtOAc (200 mL). The combined organics were washed with brine (200 mL), dried ($MgSO_4$), and concentrated in vacuo to give 163.8 g of crude product. The diastereoisomers were separated on silica gel (10−95% EtOAc in petroleum ether with 2% triethylamine) to afford 3-(4-(*tert*-butyldimethylsilyl)-3,5-difluoro-6-((*S*)-3-((*R*)-3-methyl-2-(trimethylsilyloxy)butan-2-yl)piperazin-1-yl)pyridin-2-yl)-1*H*-pyrazolo[3,4-*b*]pyridine as an orange foam (60.1 g, 69%). ^{1}H NMR (CDCl$_3$) δ 0.01 (9H, s), 0.32 (6H, s), 0.76−0.84 (9H, m), 1.11 (4H, m), 1.45 (4H, m), 1.72 (1H, m), 1.90 (1H, s), 2.61 (1H, m), 2.74 (2H, m), 2.97 (1H, m), 3.11 (1H, m), 3.64 (1H, m), 3.82 (1H, m), 3.96 (1H, m), 7.09 (1H, m), 8.48 (1H, m), 8.74 (1H, m), 11.31 (1H, brs); ^{19}F NMR (decoupled) δ −113.45, −108.39. MS *m*/*z*: 589.2 (M + H)$^+$.

Step 5. 3-(4-(*tert*-Butyldimethylsilyl)-3,5-difluoro-6-((*S*)-3-((*R*)-3-methyl-2-(trimethylsilyloxy)butan-2-yl)piperazin-1-yl)pyridin-2-yl)-1*H*-pyrazolo[3,4-*b*]pyridine (60 g, 101.9 mmol) was dissolved in THF (216.0 mL) at room temperature. A solution of tetrabutylammonium fluoride in THF (214.0 mmol. 214.0 mL of 1 M) was added dropwise via cannula to the brown solution over 45 min. The reaction mixture was stirred for 18 h at room temperature. The mixture was diluted with EtOAc (600 mL) and washed with saturated aqueous $NaHCO_3$ (100 mL, then 2 × 200 mL). The organic phase was further washed with a 2:3 mixture of saturated brine/water (100 mL) until no remaining Bu_4N^+ salts were observed. The organic phase was dried ($MgSO_4$) and concentrated in vacuo. The solid was triturated with diethyl ether, filtered, and dried to give an orange-brown solid (34.5 g). The solid was recrystallized from isopropanol to afford compound **26** as a beige solid (28.3 g, 69%). ^{1}H NMR (DMSO-*d*$_6$) δ 0.84 (3H, d), 0.90 (3H, d), 1.06 (3H, s), 1.83 (2H, m), 2.74 (2H, d), 2.85 (2H, d), 3.09 (1H, d), 3.78 (1H, d), 4.04 (1H, d), 4.13 (1H, s), 7.30 (1H, dd), 7.92 (1H, dd), 8.60 (1H, dd), 8.77 (1H, dd), 13.99 (1H, NH); ^{19}F NMR (decoupled) δ −128.5, −124.1. MS *m*/*z*: 403.2 (M + H)$^+$.

Anal. Calcd for $C_{20}H_{24}F_2N_6O$: C, 59.69%; H, 6.01%; N, 20.87%. Found: C, 59.69%; H, 5.96%; N, 20.95%.

(R)-2-((S)-4-(3-Chloro-5-fluoro-6-(1H-pyrazolo[3,4-b]pyridin-3-yl)pyridin-2-yl)piperazin-2-yl)-3-methylbutan-2-ol (27). *Step 1.* A solution of diisopropylamine (78.52 g, 108.8 mL, 776.0 mmol) in THF (1.21 L) was cooled to −20 °C. *n*-BuLi (2.5 M in hexanes) (298.4 mL of 2.5 M, 746.1 mmol) was added dropwise via cannula over 30 min at such a rate that the temperature was kept below −15 °C. Once the addition was completed, the cooling bath was removed and the reaction mixture was allowed to warm to 0 °C. The reaction mixture was stirred for 15 min at 0 °C and recooled to −78 °C. 3-Chloro-2,5-difluoropyridine (95.96 g, 596.9 mmol) was added dropwise via cannula over 20 min at such a rate that the temperature was kept below −70 °C. The reaction mixture was stirred for 45 min at −78 °C. A solution of *tert*-butylchlorodimethylsilane (117.0 g, 776.0 mmol) in THF (133.9 mL) was added via cannula at such a rate to maintain the reaction temperature below −70 °C. The reaction mixture was stirred at −78 °C for 90 min. A saturated aqueous NH$_4$Cl solution (300 mL) was added, and the reaction mixture was allowed to warm to room temperature. The reaction mixture was diluted with water (200 mL) and saturated aqueous NaHCO$_3$ (500 mL) and extracted with EtOAc (1.5 L and 500 mL). The combined organics were washed with brine (400 mL), dried (MgSO$_4$), and concentrated in vacuo to an oil (187 g). The crude material was purified by flash column chromatography (CombiFlash Companion XL, 1.5 kg silica column, 0.5−10% EtOAc in petroleum ether) to afford 4-(*tert*-butyldimethylsilyl)-3-chloro-2,5-difluoropyridine as a pale yellow oil (113.8 g, 72%). ^{1}H NMR (CDCl$_3$) δ 0.46 (6H, d), 0.93 (9H, s), 7.84 (1H, d); ^{19}F NMR (decoupled) δ −112.8, −74.6. MS *m/z*: 264.1 (M + H)$^+$.

Step 2. A solution of diisopropylamine (52.41 g, 72.59 mL, 517.9 mmol) in THF (967.3 mL) was cooled to −20 °C. *n*-BuLi (2.5 M in hexane) (198.5 mL of 2.5 M, 496.3 mmol) was added dropwise over 15 min via cannula, maintaining the internal temperature below −15 °C. The solution was warmed to 0 °C and then immediately recooled to −90 °C. A solution of 4-(*tert*-butyldimethylsilyl)-3-chloro-2,5-difluoropyridine (113.84 g, 431.6 mmol) in THF (85 mL) was added dropwise over 20 min via cannula at such a rate that the internal temperature was kept below −85 °C. The reaction mixture was stirred at −85 °C for 1 h. A solution of 2-fluoro-*N*-methoxy-*N*-methylpyridine-3-carboxamide (91.40 g, 496.3 mmol) in THF (85 mL) was added dropwise over 15 min via cannula at such a rate that the internal temperature was kept below −85 °C. The mixture was stirred at −85 °C for 90 min. The cooling bath was removed and the mixture allowed to warm to −50 °C. A saturated aqueous NH$_4$Cl solution (400 mL) was added, and the mixture was allowed to warm to room temperature. The mixture was diluted with EtOAc (1.5 L). The aqueous layer was separated and extracted with more EtOAc (300 mL). The combined organics were washed with brine (300 mL), dried (MgSO$_4$), and concentrated in vacuo. The crude material was purified by flash chromatography (CombiFlash Companion XL, 1.5 kg silica gel, 0.5−10% EtOAc in petroleum ether, 0−50% EtOAc in petroleum ether) to afford (4-(*tert*-butyldimethylsilyl)-5-chloro-3,6-difluoropyridin-2-yl)(2-fluoropyridin-3-yl)methanone as a yellow oil which solidified on standing (159.6 g, 95%). ^{1}H NMR (CDCl$_3$) δ 0.60 (6H, d), 1.07 (9H, s), 7.47 (1H, m), 8.33 (1H, m), 8.52 (1H, m); ^{19}F NMR (decoupled) δ −107.2, −72.4, −61.8. MS *m/z*: 387.1 (M + H)$^+$.

Step 3. (4-(*tert*-Butyldimethylsilyl)-5-chloro-3,6-difluoropyridin-2-yl)(2-fluoropyridin-3-yl)methanone (294.86 g, 762.2 mmol) was dissolved in dioxane (2.2 L), and calcium carbonate (152.5 g, 1.52 mol) was added. The reaction mixture was cooled in an ice bath, and hydrazine hydrate (190.8 g, 185.4 mL, 3.811 mol) was added dropwise over 15 min via cannula to the yellow suspension, keeping the internal temperature below 10 °C. The resulting mixture was allowed to warm to ambient temperature and stirred at room temperature for 18 h. The reaction mixture was filtered through a pad of Celite, washing with DCM (2.5 L). Water (400 mL) was added to the filtrate followed by a saturated solution of sodium bicarbonate (400 mL). The organic layer was separated and washed again with a saturated aqueous sodium bicarbonate solution (350 mL). The combined aqueous layers were

extracted with DCM (2 × 400 mL). The combined organics were dried (MgSO$_4$), filtered, and concentrated in vacuo. The resulting solid was slurried in petroleum ether, filtered, and dried (81 g). The Celite was further washed with DCM/MeOH 7:1 (3 × 800 mL) and with 4 L of DCM/MeOH 4:1 until no remaining compound was observed on TLC. The filtrate was concentrated in vacuo. The residual solid was triturated with petroleum ether as described above (185 g). The solids were combined and dried at 40 °C under vacuum to afford 3-(4-(*tert*-butyldimethylsilyl)-5-chloro-3,6-difluoropyridin-2-yl)-1H-pyrazolo[3,4-b]pyridine as an off-white solid (260.5 g, 89%). ^{1}H NMR (CDCl$_3$) δ 0.63 (6H, d), 1.07 (9H, s), 7.44 (1H, m), 8.76 (1H, m), 9.07 (1H, m), 13.31 (1H, NH); ^{19}F NMR (decoupled) δ −104.7, −73.8. MS *m/z*: 381.1 (M + H)$^+$.

Step 4. 3-(4-(*tert*-Butyldimethylsilyl)-5-chloro-3,6-difluoropyridin-2-yl)-1H-pyrazolo[3,4-b]pyridine (132.7 g, 348 mmol) was dissolved in anhydrous THF (265 mL). Imidazol-1-yl(trimethyl)silane (254 mL) was added followed by a mixture of (R)-3-methyl-2-((S)-piperazin-2-yl)butan-2-ol and (R)-3-methyl-2-((R)-piperazin-2-yl)-butan-2-ol (90 g, 522 mmol). The mixture was divided into four glass pressure vessels, and the sealed containers were heated and stirred at 95 °C for 48 h. The crude mixtures were cooled, combined, and diluted with EtOAc (1.7 L). The solution was washed with saturated NaHCO$_3$ (2 × 500 mL). The combined aqueous layers were extracted with EtOAc (500 mL). The combined organics were washed with brine (500 mL), dried (MgSO$_4$), filtered, and concentrated in vacuo. The diastereoisomers were separated by flash chromatography (silica gel, 10−100% EtOAc containing 2% triethylamine in petroleum ether) to afford 3-(4-(*tert*-butyldimethylsilyl)-5-chloro-3-fluoro-6-((S)-3-((R)-3-methyl-2-(trimethyl silyl oxy)butan-2-yl)piperazin-1-yl)-pyridin-2-yl)-1H-pyrazolo[3,4-b]pyridine as a yellow foam (125.3 g, 59%). ^{1}H NMR (CDCl$_3$) δ 0.01 (9H, s), 0.42 (6H, s), 0.78−0.89 (15H, m), 1.09−1.13 (3H, m), 1.74 (1H, m), 2.61 (1H, m), 2.80−2.99 (4H, m), 3.12 (1H, m), 3.45 (1H, d), 3.69 (1H, d), 7.12 (1H, m), 8.55 (1H, m), 8.81 (1H, m), 12.75 (1H, brs); ^{19}F NMR (decoupled) δ −108.9. MS *m/z*: 605.6 (M + H)$^+$.

Step 5. 3-(4-(*tert*-Butyldimethylsilyl)-5-chloro-3-fluoro-6-((S)-3-((R)-3-methyl-2-(trimethylsilyloxy)butan-2-yl)piperazin-1-yl)pyridin-2-yl)-1H-pyrazolo[3,4-b]pyridine (125 g, 206.5 mmol) was dissolved in THF (450 mL) at room temperature. Tetrabutylammonium fluoride (433.6 mL of 1 M THF solution, 433.6 mmol) was added dropwise via cannula to the yellow solution. The mixture was stirred for 48 h. The mixture was diluted with EtOAc (1.5 L) and washed with a 1:1 mixture of saturated aqueous NaHCO$_3$ and water (3 × 600 mL). The combined aqueous layers were extracted with EtOAc (2 × 600 mL), and the organic phase was washed with brine (600 mL), dried (MgSO$_4$) and partially concentrated in vacuo until the title product began to precipitate. A few drops of methanol were added, and the mixture was stirred at room temperature for 18 h. The product was filtered, rinsed with a minimum of EtOAc and petroleum ether, and dried under vacuum for 24 h (40 °C and 1.5 mbar) to afford compound **27** as a white solid (73.1 g, 84%). Mp: 217−218 °C. $[\alpha]_D^{19}$ −54.8 (*c* 1.0, EtOH). ^{1}H NMR (DMSO-*d*$_6$) δ 0.91 (3H, d), 0.94 (3H, d), 1.10 (3H, s), 1.83 (2H, m), 2.72 (1H, t), 2.80−2.94 (3H, m), 3.14−3.17 (1H, m), 3.62 (1H, d), 3.88 (1H, d), 4.14 (1H, s), 7.37 (1H, dd), 8.16 (1H, d), 8.65 (1H, dd), 8.86 (1H, dd), 14.12 (1H, NH); ^{19}F NMR (decoupled) δ −127.9. MS *m/z*: 419.1 (M + H)$^+$. >98% ee (Minigram SFC, ODH 250 mm × 10 mm, 20% MeOH (0.1% TEA), 5 mg/mL). Anal. Calcd for $C_{20}H_{24}ClFN_6O$: C, 57.35%; H, 5.77%; N, 20.06%. Found: C, 57.42%; H, 5.94%; N, 19.92%.

Kinase Inhibition Assays. Compounds were screened for their ability to inhibit PKCθ in a radioactive-phosphate incorporation assay using full-length recombinant PKCθ enzyme.

Assays were carried out in a 96-well plate containing 100 mM HEPES (pH 7.5), 10 mM MgCl$_2$, 25 mM NaCl, 0.1 mM EDTA, 0.01% Brij, 2 mM DTT, 0.002% Triton X-100, 200 µg/mL phosphatidylserine, 20 µg/mL diacylglycerol, 150 µM substrate peptide (ERMRPRKRQGSVRRRV), 0.5 nM PKCθ (Invitrogen, Madison, WI), and 240 µM ATP (ATP K_m = 40 µM) in a final volume of 100 µL. Assays were performed at 25 °C in the presence of 23 nCi/µL [γ-^{33}P]ATP (Perkin-Elmer, Beconsfield, U.K.). Serial

dilutions of inhibitors were prepared in DMSO, and the reaction was initiated by the addition of ATP.

The reaction was stopped after 60 min by the addition of 100 μL of 100 mM phosphoric acid, and a phosphocellulose 96-well plate (Millipore, catalog no. MAPHNOB) was washed with 200 μL of 100 mM phosphoric acid prior to the addition of the stopped reaction mixture (120 μL). The plate was left to soak for at least 30 min prior to washing (4 × 200 μL of 100 mM phosphoric acid). After it was dried, 100 μL of Optiphase "SuperMix" liquid scintillation cocktail (Perkin-Elmer) was added to the well. Initial rate data were determined from the level of ^{33}P incorporation measured using a 1450 MicroBeta liquid scintillation counter, Wallac.

Compounds were screened for their ability to inhibit PKCδ or PKCα in a spectrophotometric assay using full-length, recombinant enzyme.

Assays were carried out in a 384-well plate containing 100 mM HEPES (pH 7.5), 10 mM MgCl$_2$, 25 mM NaCl, 0.1 mM EDTA, 0.01% Brij, 100 μM CaCl$_2$ (PKCα only), 2 mM DTT, 0.002% Triton X-100, 200 μg/mL phosphatidylserine (100 μg/mL for PKCα), 20 μg/mL diacylglycerol, 150 μM substrate peptide (ERMRPRKR-QGSVRRRV(PKCδ); RRRRRKGSFKRKA(PKCα)), 360 μM NADH, 3 mM phosphoenolpyruvate, 70 μg/mL pyruvate kinase, 24 μg/mL lactate dehydrogenase with 46 nM PKCδ or 4.5 nM PKCα, and 150 μM ATP (K_m = 50 μM) or 130 μM ATP (K_m = 45 μM), respectively, in a final volume of 33 μL. Serial dilutions of inhibitors were prepared in DMSO, and the reaction was initiated by the addition of ATP.

Initial rate data were determined from the rate of change of absorbance at 340 nM (corresponding to stoichiometric consumption of NADH) using a Molecular Devices Spectramax plate reader (Sunnyvale, CA) over 15 min at 25 °C.

K_i values were calculated by fitting initial rate data to the model for competitive tight binding inhibition using the Prism software package (Prism 4.0a, Graphpad Software, San Diego, CA).

PBMC T Cell IL-2 Assays. PBMCs were prepared from human blood, washed, and adjusted to a cell density of 5 × 10^5 cells/mL in complete medium, and an amount of 100 μL was added to wells of 96-well Immunosorp plates (Nunc), containing immobilized anti-human CD3 (1.5 μg/mL, Serotec, U.K.), anti-human CD28 (1 μg/mL, BD, U.K.), and serial dilutions of PKCθ inhibitors or DMSO vehicle. The cell assay plates were incubated for 24 h in a humidified incubator in 5% CO$_2$ at 37 °C. Supernatants were collected and IL-2 levels determined using a bead-based FLISA assay (Applied Biosystems, U.K.). IC$_{50}$ values were determined by nonlinear regression analysis in Prism (Graphpad Software Inc.).

WB IL-2. Human whole blood (950 μL) was dispensed into a 96-well cluster plate and 50 μL of serial dilutions of PKCθ inhibitor or DMSO vehicle added and incubated for 1 h on a plate shaker. The whole blood was treated with 25 μL/well PHA solution (Gibco, U.K.) and incubated in a shaking incubator at 37 °C for 6 h. Cells were pelleted by centrifuging the plates. The supernatant was collected, and IL-2 levels were determined using a human IL-2 ELISA (R&D Systems, U.K.).

SEB-Induced IL-2 Release. All procedures described below were performed in accordance with the Animals (Scientific Procedures) Act 1986 and under the authority of a UK Home Office Project License. Female Balb/c mice (8 weeks old) were purchased from Harlan UK Ltd. Animals were allowed to acclimatize for at least 1 week prior to experimentation.

Compound **27** was formulated as a solution in 1% Tween 80/99% sodium citrate buffer, pH 3. All treatments were given by oral gavage and at a dose volume of 10 mL/kg. The number of animals per treatment group ranged from six to eight. A single dose of compound **27** (6.25, 12, 25, 50 mg/kg) was administered to animals. A control group received vehicle (1% Tween 80/99% sodium citrate buffer, pH 3). Cyclosporin A (15 mg/kg) was used as a reference compound. One hour following the administration of vehicle, cyclosporin A, or compound **27**, animals were injected intraperitoneally with SEB (10 mg in 200 μL). At 2 h later, terminal blood samples were taken and plasma was analyzed for IL-2 concentration. The concentrations of IL-

2 in plasma samples were determined using a sandwich enzyme immunoassay technique.

Statistical analysis of data was conducted with a one-way ANOVA followed by a Dunnett's post-test. Statistical significance was defined as $p < 0.05$.

Molecular Modeling. The crystal structure of human PKCθ in complex with 3-(8-((dimethylamino)methyl)-6,7,8,9-tetrahydropyrido[1,2-a]indol-10-yl)-4-(1-methyl-1H-indol-3-yl)-1H-pyrrole-2,5-dione solved at a resolution of 2.32 Å was downloaded from the Protein Data Bank (PDB code 2JED; Stark et al., unpublished study). This structure shows the C-terminus in close contact with the ligand. When this structure was overlaid with other kinase crystal structures, an unusual conformation of Phe664 was observed (this conformation is most likely induced by the ligand crystallized, and it is not usually observed among kinases structures). Therefore, this structure, in absence of the ligand, was energy minimized using the MMFF94x force field within MOE (version 2010.10, Chemical Computing Group, Montreal, Canada) and a conformation for Phe664 similar to other kinases was obtained and this new minimized structure was used for docking.

A protein model of PKCδ was created using the homology modeling tool within MOE. In order to create this protein model, the sequence of PKCδ was retrieved from UNIPROT (UNIPROT code Q05655; The UniProt Consortium, 2011) and homology modeling was carried out using as template the minimized PKCθ crystal structure described above. Medium model refinements were applied during the protein model generation. The sequence identity percentage between human PKCθ and human PKCδ for the kinase domain is approximately 72%.

Molecular docking was performed using "Extra Precision (XP) Glide" (Schrödinger, New York, U.S.; Friesner et al., 2006). The docking algorithm performs a conformational analysis of the ligand in the kinase active site. In particular, the XP scoring function considers hydrophobic packing and presence of hydrogen bonds in hydrophobic environments that are important features in predicting protein−ligand interactions in the active sites of kinases.

■ ASSOCIATED CONTENT

Ⓢ Supporting Information

Additional experimental details. This material is available free of charge via the Internet at http://pubs.acs.org.

■ AUTHOR INFORMATION

Corresponding Author

*Phone: + 44 (0) 1235 438800. E-mail: juan-miguel_jimenez@vrtx.com.

Notes

The authors declare no competing financial interest.

■ ABBREVIATIONS USED

LipE, lipophilic ligand efficiency; DAG, diacylglycerol; TCR, T cell receptor; CD28, cluster of differentiation 28; AP-1, activator protein 1; NFκB, nuclear factor κ light-chain enhancer of activated B cells; NFAT, nuclear factor of activated T cells; IL-2, interleukin 2; Bcl-xL, B-cell lymphoma, extra large; Bcl-2, B-cell lymphoma 2; Bad, Bcl-2-associated death promoter; MS, multiple sclerosis; GRL, glycine rich loop; PBMC, peripheral blood mononuclear cell

■ REFERENCES

(1) Rosse, C.; Linch, M.; Kermorgant, S.; Cameron, A. J.; Boeckeler, K.; Parker, P. J. PKC and the control of localized signal dynamics. *Nat. Rev. Mol. Cell Biol.* **2010**, *11*, 103−112.

(2) Baier, G.; Telford, D.; Giampa, L.; Coggeshall, K. M.; Baier-Bitterlich, G.; Isakov, N.; Altman, A. Molecular cloning and characterization of PKC theta, a novel member of the protein kinase C (PKC) gene family expressed predominantly in hematopoietic cells. *J. Biol. Chem.* **1993**, *268*, 4997−5004.

(3) Sun, Z.; Arendt, C. W.; Ellmeier, W.; Schaeffer, E. M.; Sunshine, M. J.; Gandhi, L.; Annes, J.; Petrzilka, D.; Kupfer, A.; Schwartzberg, P. L.; Littman, D. R. PKC-theta is required for TCR-induced NF-kappaB activation in mature but not immature T lymphocytes. *Nature* **2000**, *404*, 402−407.

(4) Pfeifhofer, C.; Kofler, K.; Gruber, T.; Tabrizi, N. G.; Lutz, C.; Maly, K.; Leitges, M.; Baier, G. Protein kinase C theta affects Ca2+ mobilization and NFAT cell activation in primary mouse T cells. *J. Exp. Med.* **2003**, *197*, 1525−1535.

(5) Manicassamy, S.; Sadim, M.; Ye, R. D.; Sun, Z. Differential roles of PKC-theta in the regulation of intracellular calcium concentration in primary T cells. *J. Mol. Biol.* **2006**, *355*, 347−359.

(6) Baier-Bitterlich, G.; Uberall, F.; Bauer, B.; Fresser, F.; Wachter, H.; Grunicke, H.; Utermann, G.; Altman, A.; Baier, G. Protein kinase C-theta isoenzyme selective stimulation of the transcription factor complex AP-1 in T lymphocytes. *Mol. Cell. Biol.* **1996**, *16*, 1842−50.

(7) Coudronniere, N.; Villalba, M.; Englund, N.; Altman, A. NF-kappa B activation induced by T cell receptor/CD28 costimulation is mediated by protein kinase C-theta. *Proc. Natl. Acad. Sci. U.S.A.* **2000**, *97*, 3394−3399.

(8) Lin, X.; O'Mahony, A.; Mu, Y.; Geleziunas, R.; Greene, W. C. Protein kinase C-theta participates in NF-kappaB activation induced by CD3-CD28 costimulation through selective activation of IkappaB kinase beta. *Mol. Cell. Biol.* **2000**, *20*, 2933−40.

(9) Bertolotto, C.; Maulon, L.; Filippa, N.; Baier, G.; Auberger, P. Protein kinase C theta and epsilon promote T-cell survival by a rsk-dependent phosphorylation and inactivation of BAD. *J. Biol. Chem.* **2000**, *275*, 37246−37250.

(10) Villalba, M.; Bushway, P.; Altman, A. Protein kinase C-theta mediates a selective T cell survival signal via phosphorylation of BAD. *J. Immunol.* **2001**, *166*, 5955−5963.

(11) Barouch-Bentov, R.; Lemmens, E. E.; Hu, J.; Janssen, E. M.; Droin, N. M.; Song, J.; Schoenberger, S. P.; Altman, A. Protein kinase C-theta is an early survival factor required for differentiation of effector CD8+ T cells. *J. Immunol.* **2005**, *175*, 5126−5134.

(12) Manicassamy, S.; Gupta, S.; Huang, Z.; Sun, Z. Protein kinase C-theta-mediated signals enhance CD4+ T cell survival by up-regulating Bcl-xL. *J. Immunol.* **2006**, *176*, 6709−6716.

(13) Berg-Brown, N. N.; Gronski, M. A.; Jones, R. G.; Elford, A. R.; Deenick, E. K.; Odermatt, B.; Littman, D. R.; Ohashi, P. S. PKCtheta signals activation versus tolerance in vivo. *J. Exp. Med.* **2004**, *199*, 743−752.

(14) Marsland, B. J.; Soos, T. J.; Spath, G.; Littman, D. R.; Kopf, M. Protein kinase C theta is critical for the development of in vivo T helper (Th)2 cell but not Th1 cell responses. *J. Exp. Med.* **2004**, *200*, 181−189.

(15) Giannoni, F.; Lyon, A. B.; Wareing, M. D.; Dias, P. B.; Sarawar, S. R. Protein kinase C theta is not essential for T-cell-mediated clearance of murine gammaherpesvirus 68. *J. Virol.* **2005**, *79*, 6808−6813.

(16) Marsland, B. J.; Nembrini, C.; Schmitz, N.; Abel, B.; Krautwald, S.; Bachmann, M. F.; Kopf, M. Innate signals compensate for the absence of PKC-{theta} during in vivo CD8(+) T cell effector and memory responses. *Proc. Natl. Acad. Sci. U.S.A.* **2005**, *102*, 14374−14379.

(17) Marsland, B. J.; Nembrini, C.; Grun, K.; Reissmann, R.; Kurrer, M.; Leipner, C.; Kopf, M. TLR ligands act directly upon T cells to restore proliferation in the absence of protein kinase C-theta signaling and promote autoimmune myocarditis. *J. Immunol.* **2007**, *178*, 3466−3473.

(18) Salek-Ardakani, S.; So, T.; Halteman, B. S.; Altman, A.; Croft, M. Differential regulation of Th2 and Th1 lung inflammatory responses by protein kinase C theta. *J. Immunol.* **2004**, *173*, 6440−6447.

(19) Salek-Ardakani, S.; So, T.; Halteman, B. S.; Altman, A.; Croft, M. Protein kinase Ctheta controls Th1 cells in experimental autoimmune encephalomyelitis. *J. Immunol.* **2005**, *175*, 7635−7641.

(20) Tan, S. L.; Zhao, J.; Bi, C.; Chen, X. C.; Hepburn, D. L.; Wang, J.; Sedgwick, J. D.; Chintalacharuvu, S. R.; Na, S. Resistance to experimental autoimmune encephalomyelitis and impaired IL-17 production in protein kinase C theta-deficient mice. *J. Immunol.* **2006**, *176*, 2872−2879.

(21) Anderson, K.; Fitzgerald, M.; Dupont, M.; Wang, T.; Paz, N.; Dorsch, M.; Healy, A.; Xu, Y.; Ocain, T.; Schopf, L.; Jaffee, B.; Picarella, D. Mice deficient in PKC theta demonstrate impaired in vivo T cell activation and protection from T cell-mediated inflammatory diseases. *Autoimmunity* **2006**, *39*, 469−478.

(22) Healy, A. M.; Izmailova, E.; Fitzgerald, M.; Walker, R.; Hattersley, M.; Silva, M.; Siebert, E.; Terkelsen, J.; Picarella, D.; Pickard, M. D.; LeClair, B.; Chandra, S.; Jaffee, B. PKC-theta-deficient mice are protected from Th1-dependent antigen-induced arthritis. *J. Immunol.* **2006**, *177*, 1886−1893.

(23) Nagahama, K.; Ogawa, A.; Shirane, K.; Shimomura, Y.; Sugimoto, K.; Mizoguchi, A. Protein kinase C theta plays a fundamental role in different types of chronic colitis. *Gastroenterology* **2008**, *134*, 459−469.

(24) Skvara, H.; Dawid, M.; Kleyn, E.; Wolff, B.; Meingassner, J. G.; Knight, H.; Dumortier, T.; Kopp, T.; Fallahi, N.; Stary, G.; Burkhart, C.; Grenet, O.; Wagner, J.; Hijazi, Y.; Morris, R. E.; McGeown, C.; Rordorf, C.; Griffiths, C. E.; Stingl, G.; Jung, T. The PKC inhibitor AEB071 may be a therapeutic option for psoriasis. *J. Clin. Invest.* **2008**, *118*, 3151−3159.

(25) Budde, K.; Sommerer, C.; Becker, T.; Asderakis, A.; Pietruck, F.; Grinyo, J. M.; Rigotti, P.; Dantal, J.; Ng, J.; Barten, M. J.; Weber, M. Sotrastaurin, a novel small molecule inhibiting protein kinase C: first clinical results in renal-transplant recipients. *Am. J. Transplant.* **2010**, *10*, 571−581.

(26) Wagner, J.; von Matt, P.; Sedrani, R.; Albert, R.; Cooke, N.; Ehrhardt, C.; Geiser, M.; Rummel, G.; Stark, W.; Strauss, A.; Cowan-Jacob, S. W.; Beerli, C.; Weckbecker, G.; Evenou, J. P.; Zenke, G.; Cottens, S. Discovery of 3-(1*H*-indol-3-yl)-4-[2-(4-methylpiperazin-1-yl)quinazolin-4-yl]pyrrole-2,5-dione (AEB071), a potent and selective inhibitor of protein kinase C isotypes. *J. Med. Chem.* **2009**, *52*, 6193−6196.

(27) Wagner, J.; von Matt, P.; Faller, B.; Cooke, N. G.; Albert, R.; Sedrani, R.; Wiegand, H.; Jean, C.; Beerli, C.; Weckbecker, G.; Evenou, J. P.; Zenke, G.; Cottens, S. Structure−activity relationship and pharmacokinetic studies of sotrastaurin (AEB071), a promising novel medicine for prevention of graft rejection and treatment of psoriasis. *J. Med. Chem.* **2011**, *54*, 6028−6039.

(28) Subrath, J.; Wang, D.; Wu, B.; Niu, C.; Boschelli, D. H.; Lee, J.; Yang, X.; Brennan, A.; Chaudhary, D. C-5 Substituted heteroaryl 3-pyridinecarbonitriles as PKCtheta inhibitors: part I. *Bioorg. Med. Chem. Lett.* **2009**, *19*, 5423−5425.

(29) Prashad, A. S.; Wang, D.; Subrath, J.; Wu, B.; Lin, M.; Zhang, M. Y.; Kagan, N.; Lee, J.; Yang, X.; Brennan, A.; Chaudhary, D.; Xu, X.; Leung, L.; Wang, J.; Boschelli, D. H. C-5 substituted heteroaryl-3-pyridinecarbonitriles as PKCtheta inhibitors: part II. *Bioorg. Med. Chem. Lett.* **2009**, *19*, 5799−5802.

(30) Cole, D. C.; Asselin, M.; Brennan, A.; Czerwinski, R.; Ellingboe, J. W.; Fitz, L.; Greco, R.; Huang, X.; Joseph-McCarthy, D.; Kelly, M. F.; Kirisits, M.; Lee, J.; Li, Y.; Morgan, P.; Stock, J. R.; Tsao, D. H.; Wissner, A.; Yang, X.; Chaudhary, D. Identification, characterization and initial hit-to-lead optimization of a series of 4-arylamino-3-pyridinecarbonitrile as protein kinase C theta (PKCtheta) inhibitors. *J. Med. Chem.* **2008**, *51*, 5958−5963.

(31) Dushin, R. G.; Nittoli, T.; Ingalls, C.; Boschelli, D. H.; Cole, D. C.; Wissner, A.; Lee, J.; Yang, X.; Morgan, P.; Brennan, A.; Chaudhary, D. Synthesis and PKCtheta inhibitory activity of a series of 4-

indolylamino-5-phenyl-3-pyridinecarbonitriles. *Bioorg. Med. Chem. Lett.* **2009**, *19*, 2461−2463.

(32) Wu, B.; Boschelli, D. H.; Lee, J.; Yang, X.; Chaudhary, D. Second generation 4-(4-methyl-1*H*-indol-5-ylamino)-2-phenylthieno-[2,3-*b*]pyridine-5-carbonitrile PKCtheta inhibitors. *Bioorg. Med. Chem. Lett.* **2009**, *19*, 766−769.

(33) Boschelli, D. H.; Wu, B.; Barrios Sosa, A. C.; Chen, J.; Asselin, M.; Cole, D. C.; Lee, J.; Yang, X.; Chaudhary, D. Synthesis and PKCtheta inhibitory activity of a series of 4-(indol-5-ylamino)thieno-[2,3-*b*]pyridine-5-carbonitriles. *Bioorg. Med. Chem. Let.* **2008**, *18*, 2850−2853.

(34) Nathan Tumey, L.; Boschelli, D. H.; Lee, J.; Chaudhary, D. 2-Alkenylthieno[2,3-*b*]pyridine-5-carbonitriles: potent and selective inhibitors of PKCtheta. *Bioorg. Med. Chem. Lett.* **2008**, *18*, 4420−4423.

(35) Boschelli, D. H.; Wang, D.; Prashad, A. S.; Subrath, J.; Wu, B.; Niu, C.; Lee, J.; Yang, X.; Brennan, A.; Chaudhary, D. Optimization of 5-phenyl-3-pyridinecarbonitriles as PKCtheta inhibitors. *Bioorg. Med. Chem. Lett.* **2009**, *19*, 3623−3626.

(36) Boschelli, D. H.; Subrath, J.; Niu, C.; Wu, B.; Wang, Y.; Lee, J.; Brennan, A.; Ho, M.; Deng, B.; Yang, X.; Xu, X.; Leung, L.; Wang, J.; Atherton, J.; Chaudhary, D. Optimization of 5-vinylaryl-3-pyridine-carbonitriles as PKCtheta inhibitors. *Bioorg. Med. Chem. Lett.* **2010**, *20*, 1965−1968.

(37) Niu, C.; Boschelli, D. H.; Tumey, L. N.; Bhagirath, N.; Subrath, J.; Shim, J.; Wang, Y.; Wu, B.; Eid, C.; Lee, J.; Yang, X.; Brennan, A.; Chaudhary, D. First generation 5-vinyl-3-pyridinecarbonitrile PKCtheta inhibitors. *Bioorg. Med. Chem. Lett.* **2009**, *19*, 5829−5832.

(38) Shim, J.; Eid, C.; Lee, J.; Liu, E.; Chaudhary, D.; Boschelli, D. H. Synthesis and PKCtheta inhibitory activity of a series of 5-vinyl phenyl sulfonamide-3-pyridinecarbonitriles. *Bioorg. Med. Chem. Lett.* **2009**, *19*, 6575−6577.

(39) Cywin, C. L.; Dahmann, G.; Prokopowicz, A. S., 3rd; Young, E. R.; Magolda, R. L.; Cardozo, M. G.; Cogan, D. A.; Disalvo, D.; Ginn, J. D.; Kashem, M. A.; Wolak, J. P.; Homon, C. A.; Farrell, T. M.; Grbic, H.; Hu, H.; Kaplita, P. V.; Liu, L. H.; Spero, D. M.; Jeanfavre, D. D.; O'Shea, K. M.; White, D. M.; Woska, J. R., Jr.; Brown, M. L. Discovery of potent and selective PKC-theta inhibitors. *Bioorg. Med. Chem. Lett.* **2007**, *17*, 225−230.

(40) Boschelli, D. H. Small molecule inhibitors of PKCTheta as potential antiinflammatory therapeutics. *Curr. Top. Med. Chem.* **2009**, *9*, 640−654.

(41) Jimenez, J.-M.; Davis, J. C.; Boyall, D.; Fraysee, D.; Knegtel, R.; Settimo, L.; Young, S.; Bolton, C.; Chiu, P.; Curnock, A.; Rasmussen, R.; Tanner, A.; Ager, I. Structure-based optimization of amino-pyridines as PKCθ inhibitors. *Bioorg. Med. Chem. Lett.* **2012**, *22*, 4645−4649.

(42) Leeson, P. D.; Springthorpe, B. The influence of drug-like concepts on decision-making in medicinal chemistry. *Nat. Rev. Drug Discovery* **2007**, *6*, 881−890.

(43) Mecklenbrauker, I.; Saijo, K.; Zheng, N. Y.; Leitges, M.; Tarakhovsky, A. Protein kinase Cdelta controls self-antigen-induced B-cell tolerance. *Nature* **2002**, *416*, 860−865.

(44) Miyamoto, A.; Nakayama, K.; Imaki, H.; Hirose, S.; Jiang, Y.; Abe, M.; Tsukiyama, T.; Nagahama, H.; Ohno, S.; Hatakeyama, S.; Nakayama, K. I. Increased proliferation of B cells and auto-immunity in mice lacking protein kinase C delta. *Nature* **2002**, *416*, 865−869.

(45) Gill, A. L.; Verdonk, M.; Boyle, R. G.; Taylor, R. A comparison of physicochemical property profiles of marketed oral drugs and orally bioavailable anti-cancer protein kinase inhibitors in clinical development. *Curr. Top. Med. Chem.* **2007**, *7*, 1408−1422.

(46) Rummel, G.; Stark, W.; Strauss, A.; Wagner, J. Three Dimensional Structure of the Catalytic Domain of Protein C theta, Methods and Use Thereof. PCT Int. Appl. WO2004076654, 2004.